578571

Progress Report on the MgO Hydration and Carbonation Study at SNL WIPP Geochemistry

Revision 0

Kevins Rhino, Isaac Foli, Jay Jang

Organization 08882

Sandia National Laboratories

Carlsbad, New Mexico, U.S.A.

WIPP:4.4.2.2.1:TD:QA-L:RECERT:543889

Information Only

16 APPROVALS

Authored by:	Kevins Rhino		11/21/2022
	Print Name	Signature	Date
Authored by:	Isaac Foli	Kevins Rhino for	12/7/2022
	Print Name	Signature	Date
Authored by:	Jay Jang		11/21/2022
	Print Name	Signature	Date
Reviewed by:	Martin Nemer	Shelly R. Nielsen for	12-7-2022
	Print Name Technical Reviewer	Signature	Date
Reviewed by:	Shelly Nielsen	Shelly R. Nielsen	11-28-2022
	Print Name Quality Assurance Reviewer	Signature	Date
Approved by:	Chammi Miller	Chaani Miller	11/21/22
	Print Name Management Reviewer	Signature	Date

17

Information Only

I. INTRODUCTION

I.1. Revision History

This is Revision 0 of this report. Revision n ($n \geq 1$) will retain the outline of Revision n-1 and present detailed summaries of new tasks completed by the time of release of Revision n.

I.2. Current Status

Magnesium oxide (MgO)[1], is the only engineered barrier currently emplaced in the Waste Isolation Pilot Plant (WIPP) whose function is to sequester CO_2. The EPA specified MgO as the only engineered barrier in the WIPP disposal system that meets the assurance requirement in the certification rulemaking (U.S. EPA 1998), which makes the MgO an essential component of the certified design of the repository.

Even though it is not part of its primary function as the engineered barrier, MgO is expected to sequester H_2O (and CO_2). Due to the key role hydration and carbonation of MgO it is necessary to study the rates and mechanisms of MgO hydration and carbonation in the WIPP relevant environments.

SNL WIPP Geochemistry is evaluating the hydration and carbonation rates of MgO obtained from Martin Marietta Magnesia Specialties, LLC (referred to as "MM MgO" hereafter). A series of experiments were developed to investigate the long-term inundated hydration of MM MgO in GWB and ERDA-6 brines. A Loss on Ignition (LOI) method was carried out under TP 00-07 (Revision 2 by Snider and Xiong, 2002; Revision 3 by Snider et al., 2004), TP 06-03 (Revision 0 by Deng et al., 2006a; Revision 1 by Deng et al., 2007a) and AP-108 (Revision 0 by Nowak et al., 2003; Revision 1 by Deng, 2010).

Wall (2005) and Deng et al (2006b, 2007b, 2009) characterized MgO particles and hydrated samples at high temperature in DI water. The studies were carried out in order to study hydration mechanism. The authors highlighted that different mechanism may occur during hydration and may depend on particle size. While the studies provided important insight on mechanisms and model reaction, they were performed at high temperature. The experiments were performed as such to accelerate the hydration rate and to reduce the experimental time to a feasible laboratory scale. However, high temperature experiments need validation studies to be applicable for WIPP relevant conditions.

[1] Mineralogical name: periclase

Information Only

TP 06-03 (Deng et al., 2007a) prescribed the use of GWB and ERDA-6; brines composed of multiple components reactive to MgO(s). Those experimental results contained products of parallel reactions ($Mg_2Cl(OH)_3.4H_2O$(s) known as Mg-phase-3[2] and $Mg_3Cl(OH)_5.4H_2O$(s) known as Mg-phase-5 (Wall, 2005)) forming from hydroxo-chloridization (Xiong et al., 2010) in addition to hydration products.

Such phases contain a component of water in their structure (OH^-), as well as crystalline water in the form of H_2O. The water molecule or component of water may or may not remain in those phases after heating at 150°C. Additionally, the chloride in their structure may or may not interfere with the conversion back to MgO(s) upon the heating at 800°C. Formation of phases other than $Mg(OH)_2$(s) (brucite) would make it difficult, if not impossible, to attribute the mass loss measured by the LOI method entirely to the mass of water associated with the MgO(s)/$Mg(OH)_2$(s) conversion.

SNL WIPP Geochemistry has decided to take a sequential and analytical approach to determine the rates of reactions that MgO(s) would experience when placed in the WIPP-relevant conditions. The reactions include hydration, chloridization, carbonation, and mix between those processes (hydroxo-carbonation, hydroxo-chloridization and hydroxy-chloride-carbonation). Each reaction will be investigated as independently from each other as possible. After the rates and mechanisms of each reaction is elucidated the previously obtained experimental results will benefit from a more complete and comprehensive analysis.

This report documents the interim results of MgO(s) hydration in water. This report is a deviation from the existing AP-108 Rev 1 (Deng, 2010) carried out under TP 06-03 Rev 1 (Deng et al., 2007a) due to the fact experiments were performed using DI water rather than WIPP relevant brines. It is important to understand hydration reactions in DI-water as a baseline to understand hydration complexity in brine solutions. 4751[-

II. HYDRATION EXPERIMENTS

Of the two hydration modes described by the WIPP conceptual model (inundated hydration and hydration by water vapor), only samples of inundated hydration will be dealt in this revision. As explained in the previous section, SNL WIPP Geochemistry is approaching current and future experimental designs using simple systems to quantify the mechanisms that play a key role in more complicated systems at high ionic strength, multiple chemical components, and competing reaction pathways (WIPP relevant brines). The proposed future experiments to examine the hydration as well as

[2] Mineral phase : Korshunovskite

Information Only

the parallel reactions are listed in Section II.2 (Table II-10). All associated files are archived at CVS/CVSLIB/WIPP_EXTERNAL/AP108_2022

II.1. MgO(s) - H_2O

The MgO(s) - H_2O experiment is in progress. This section reports the interim results of the MgO hydration experiment in DI water.

The data are included in Scientific Notebook WIPP-MM-MgO-23 (page 69 to 80).

II.1.1. Chemical System

This experiment used the non-pure MgO(s), denoted MM MgO. The MM MgO was obtained from WIPP (NWP)[3] on 2022/02/17 and was inundated with DI water. The three system components are Mg^{+2}, H^+, and H_2O. Effects of the impurities in the MM MgO on the hydration rate are not considered and remain an unquantified source of uncertainty (Deng et al., 2009; Amaral et al., 2010) (Excerpt II-1).

[3] Nuclear Waste Partnership

Information Only

Excerpt II-1. Part of MM MgO composition Certificate (MagChem 10) as provided by Martin Marietta Magnesia Specialties LLC (Martin Marietta Magnesia Specialties LLC, ERMS 544635)

DESCRIPTION

MagChem® 10 are high purity technical grades of magnesium oxide processed from magnesium-rich brine. They have relatively high density and low reactivity. The granular grades are essentially dust free.

USES

Milled MagChem 10 grades have a combination of low reactivity, high purity and fine particle size, which makes them suitable for the production of magnesium salts, particularly in reaction with strong acids. Milled MagChem 10 grades also find applications in fiberglass, aluminum metal processing and fuel additives. Screened MagChem 10 products are widely used as a raw material in manufacturing refractories and ceramic products.

COMPOSITION

	Typical	Specifications
Magnesium Oxide (MgO), %	98.2	97.0 min.
Calcium Oxide (CaO), %	0.9	1.0 max.
Silicon Oxide (SiO_2), %	0.4	0.5 max.
Iron Oxide (Fe_2O_3), %	0.2	0.3 max.
Aluminum Oxide (Al_2O_3), %	0.1	0.2 max.
Chloride (Cl), %	0.01	0.02 max.
Sulfate (SO_3), %	0.01	0.02 max.
Loss on Ignition, %	0.25	0.5 max.

MagChem 10 grades are available in a wide variety of screened and milled sizes, from a powder minus 325 mesh to a granular ½" X 6 mesh. Loose bulk densities range from 65 to 120 lb/ft³.

Screened Grades	Top Size		Bottom Size	
Grade	% Passing, min.		% Passing, max.	
½ X 6	95	-½ inch	5	-6 mesh
6 X 16	98	-6 mesh	10	-16 mesh
12 X 40	95	-12 mesh	10	-40 mesh
PR-30	98	-16 mesh	15	-100 mesh
-60	85	-60 mesh		N/A

Milled Grades	Top Size		Median Particle
Grade	% Passing, min.		Size, Microns
-20	96	-20 mesh	50
-40	95	-40 mesh	30
-200	95	-200 mesh	10
-325	96	-325 mesh	10
-325S	99	-325 mesh	9

PACKAGING

Available in bulk carload and truckload, 50-lb polyethylene-lined, multi-walled bags and 1000-2000-lb bulk sacks.

STORAGE

Store in dry place. Exposure to moisture may cause caking.

MM MgO is approximated by MgO(s) (periclase, formula weight is 40.31 g/mol) in the data processing and interpretation in the following sections.

II.1.2. Goals and Hypotheses

The goal of the MgO(s)-H_2O experiment is to measure the time-dependent change of mole fractions of MgO(s) (periclase) and $Mg(OH)_2$(s) (brucite) during the hydration using various techniques: LOI, XRD, SEM, and TGA. It is hypothesized that the measured mole fractions can be used to determine the inundated hydration rate of periclase.

The following hypothesis are to be tested in the MgO(s)-H_2O experiments:

H-1: The hydration of MgO(s) (periclase) in water can be described by Reaction (1), and the sole product is $Mg(OH)_2$(s) (brucite).

Information Only

$$MgO(s)\ (periclase) + H_2O(l) \rightarrow Mg(OH)_2(s)\ (brucite) \quad (1)$$

where the log of equilibrium constant of Reaction (1), denoted log K(1), is 4.37 based on CRC handbook (2003), Harvie et al. (1984), and Giauque and Archibald (1937). It is worth noting that MgO(s) chemical potential has range of values that depend on the particle surface area and the method of preparation (Taylor and Wells, 1938). The calculation of log K is performed using the dimensionless chemical potentials, $\mu°/RT$, of reactant and products using Equation (2) and (3):

$$Ln\ K = \Sigma(j \times \mu_j°/RT)_{reactants} - \Sigma(i \times \mu_i°/RT)_{products} \quad (2)$$

and

$$Log\ K = Ln\ K / 2.30 \quad (3)$$

where i and j are the stoichiometric coefficient of a product and reactant respectively, $\mu°/RT$ is the dimensionless chemical potential (with RT =2.47 kJ/mol when $\mu°$ is in kJ/mol). Calculation of the log K of Reaction (1) gives:

$$Log\ K(1) = [\mu°_{MgO(s)}/RT + \mu°_{H2O}/RT - \mu°_{Mg(OH)2(s)}/RT] / 2.30$$

$$= [-229.65 - 95.66 + 335.4] / 2.30 = 4.37 \quad (4)$$

where the values for $\mu°_{MgO(s)}/RT$ (-229.65), $\mu°_{H2O}/RT$ (-95.66), and $\mu°_{Mg(OH)2(s)}/RT$ (-335.4) are adopted from CRC handbook (2003) and Harvie et al. (1984) respectively.

H-2: It is hypothesized that, because of kinetics, Reaction (1) would not go to completion in any foreseeable future in the presence of excess water, even though the thermodynamics shows otherwise. The thermodynamics of Reaction (1) indicate that, in the presence of excess water, $Mg(OH)_2(s)$ is the stable solid phase. By the mass action law, the reaction quotient K of Reaction (1) equates to the inverse of the water activity at the equilibrium of MgO(s) and $Mg(OH)_2(s)$, denoted $\{H_2O\}_{eq}$;

$$K(1) = 1 / \{H_2O\}_{eq} = 10^{4.37}, \text{ or}$$

$$\{H_2O\}_{eq} = 10^{-4.37} \quad (5)$$

The water activity in the presence of excess water, $\{H_2O\} = 1 >> \{H_2O\}_{eq}$. Therefore, MgO(s) (periclase) is thermodynamically unstable compared to $Mg(OH)_2(s)$ (brucite), and destined to disappear to form brucite as long as the liquid water exists. The dissolved concentration of Mg^{+2},

Information Only

127 [Mg^{+2}], and pH would be in equilibrium with $Mg(OH)_2$(s) (brucite) via Reaction (6) regardless of the
128 quantity of brucite, not with MgO(s) (periclase);

129 $$Mg(OH)_2(s)\ (brucite) + 2H^+ = Mg^{+2} + 2H_2O \quad (6)$$

130 where the log K of Reaction (6) is given by log K(6) = 17.11 (Harvie et al., 1984). According to the
131 mass and charge balance for Reaction (6), the [Mg^{+2}] and pH can be approximated to [Mg^{+2}] ≈ $10^{-3.9}$
132 m = 1.3 × 10^{-4} m = 3.1 ppm and pH ≈ 10.4.

133 H-3: As demonstrated in the literature (Jander, 1927; Ginstling and Brounshtein, 1950; Layden and
134 Brindley, 1963; Bratton and Brindley, 1964; Smithson and Bakhshi, 1969; Kitamura et al., 1969;
135 Levenspiel, 1963), the hydration reaction rate can be parameterized by first order reaction kinetics,
136 demonstrated in Equation (7). Per Reaction (1), the rate of $Mg(OH)_2$(s) formation is of the inverse to
137 the rate of MgO(s) consumption. Therefore, the first order reaction rate equation can be expressed
138 as:

139 $$Rate = \frac{dX_{Mg(OH)_2(s)}}{dt} = -\frac{dX_{MgO(s)}}{dt} = k_1 \cdot X_{MgO(s)} \cdot X_{H_2O(l)} \equiv k_2 \cdot X_{MgO(s)} \quad (7)$$

140 $$k_2 \equiv k_1 \cdot X_{H_2O(l)} \quad (8)$$

141 where $X_{Mg(OH)2(s)}$ and $X_{MgO(s)}$ are the mole fractions of the formed $Mg(OH)_2$(s) (brucite, the product)
142 and the remaining MgO(s) (periclase, one of the reactants), $X_{H2O(l)}$ is the mole fraction of water, k_1
143 and k_2 are the first order reaction rate constants. $X_{H2O(l)}$ can be considered constant under the
144 experimental conditions described in Section II.1.3, where the water is added in excess. Under those
145 circumstances $X_{Mg(OH)_2(s)}$ and $X_{MgO(s)}$ can be rescaled to the moles of Mg,

146 $$X_{Mg(OH)_2(s)} + X_{MgO(s)} = 1 \quad (9)$$

147 to exclude $X_{H_2O(l)}$ from Equations (7) and (8).

148 H-4: It is hypothesized that the use of an array of particle size would allow us to differentiate the
149 hydration rate as a function of particle size using the methods employed in this study. It is
150 hypothesized that hydration rate may also be dependent of the specific surface area (SSA) of the
151 MgO(s) particles; hence the investigation of hydration rate on different particle size was conducted.
152 Depending on the outcome of the experiment, H-4 may force to reconsider the kinetic law (H-3).

Information Only

II.1.3. Reactor Preparation

The experiment was prepared by mixing 100 mL of DI water with 5 g of MM MgO (40.305 g/mol) particles weighed on a calibration-checked balance. Three replicates of each sample were created to estimate the spread of the measured mole fractions after a period of hydration. 100 mL water ≡ 100 gram water at 25°C, therefore, the moles of H_2O, i.e., n_{H2O} = (100 g) / (18.015 g/mol) = 5.550 moles H_2O. Likewise, $n_{MgO(s)}$ = (5 g) / (40.305 g/mol) = 0.124 moles MgO(s). In case of the full conversion of MgO(s) to $Mg(OH)_2$(s) via Reaction (1), the maximum water consumption would be 0.124 moles H_2O, and the remaining n_{H2O} would be 5.550 - 0.124 = 5.426 moles H_2O. More than 97% of the added water would remain in case of partial conversion, thus, $X_{H_2O(l)}$ would be considered constant, and was combined with k_1 to defined k_2 in Equations (7) and (8).

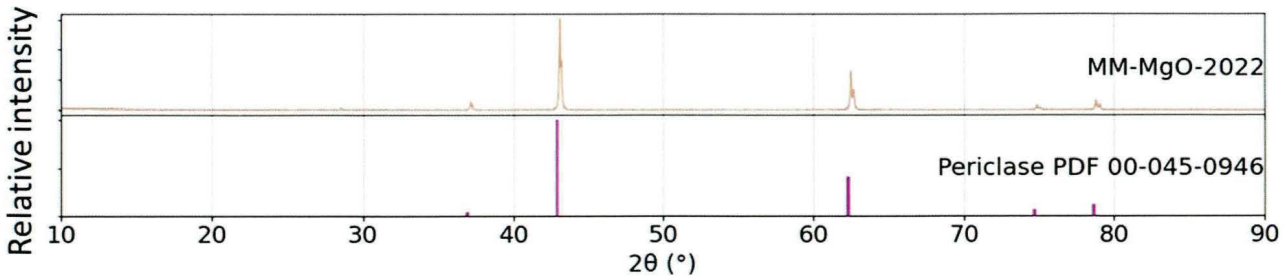
Three particle size ranges were chosen:

1) **Large size particles**: sieve sized with diameters between 1.0 and 2.0 mm,
2) **Small size particles**: sieve sized with diameters less than 75 μm, and
3) **Mixed size particles**: which is the "as received" mix from the vendor containing both small and large particles that were not sieved for size.

In total, a set of 9 reactors were prepared, i.e., triplicates per size fraction in water, and were terminated at a prescribed time of investigation.

Figure II-1 exhibits a XRD scan of the MM MgO particles SNL WIPP Geochemistry received in February 2022. The scan displays peaks that match with the MgO(s) (periclase) of Powder Diffraction File (PDF) 00-045-0946. This confirms that MM MgO consists mainly of periclase. Impurities reported in Excerpt II-1 are masked by the dominance of periclase.

Figure II-1. XRD scans of the MM MgO particle prior to the hydration (WIPP-MM-MgO-23, page 76).



Information Only

II.1.4. Data - Aqueous

10 mL aliquots are retained and kept in 15-mL tubes, for future analysis. No aqueous data was obtained for this revision.

II.1.5. Data - Solids

The day of preparation, the reactor were gently agitated by slow hand motion to ensure that every particle was hydrated. The MgO was still free-flowing particles without showing any sign of cementing or noticeable aggregation. Samples were hydrated for a predetermined length of time then immediately filtered through a Whatman 44 paper filter (particle retention in liquid: 3 μm) using a vacuum filtration device. Hydrated samples were stored in a desiccator overnight and then analyzed through the LOI method within one day to minimize the hydration by the unbound water during the storage. A source of uncertainty includes the potential loss of fine colloid particles (nano size particles and a part of the micro size particles) that were freshly hydrated into brucite. A possible avenue to investigate this uncertainty could be analyzing aliquots of unfiltered DI water from the reactors via dynamic light scattering to assess the presence and magnitude of a colloidal particle fraction. For the purpose of this Revision, we assume that the mass of analyte lost through removal of colloidal particles in the reactor liquid is negligible compared to the remaining solid phase, and that consequently the hydration results will not be influenced.

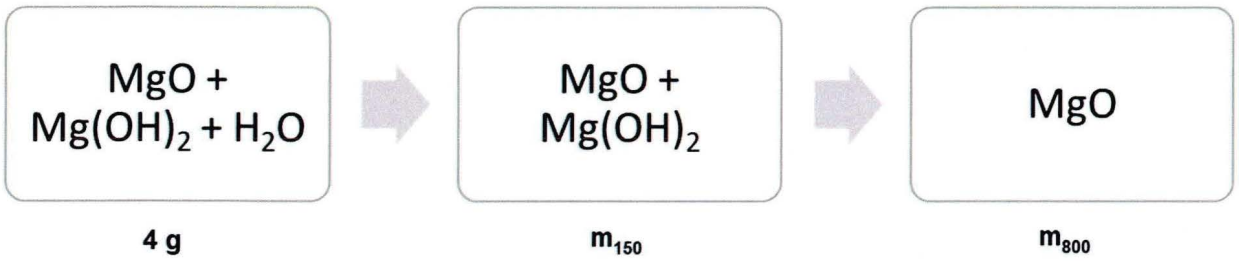
II.1.5.1. Loss of Ignition methodology (LOI)

LOI measures the mass change of a sample after it has been heated to high temperature causing some of its content to burn or to volatilize. For this study, the LOI measurement was performed as follows: 4 g of the dried hydrated samples were introduced in individual pre-weighed crucibles. As described by Deng et al. (2007a), the sample was then heated at 150°C for 2 hours in order to remove the unbound water, cooled down, and weighed. After weighing, the sample was heated to 800°C at 4°C/min– converting the $Mg(OH)_2(s)$ (brucite) back to MgO(s) (periclase) – then cooled down, and weighed. The difference between the mass of sample heated at 150°C and the mass of sample heated at 800°C is defined as the mass of water lost by reversing Reaction (1). By the 1:1 molar relation of the consumed H_2O and the formed $Mg(OH)_2(s)$ (brucite), the mass difference is converted to the moles of H_2O and $Mg(OH)_2(s)$ in the hydrated samples.

Figure II-2. A summary of the LOI process. The heating at 150°C aims at removing the unbound water and the heating to 800°C aims at converting of brucite to original

Information Only

207 periclase. The phase identifier, (s), in MgO(s) and $Mg(OH)_2$(s) is omitted for
208 simplicity.



209

210 $Mg(OH)_2$(s) (brucite) content is determined by the difference of m_{150} and m_{800}, the mass of the
211 sample after being heated at 150°C and 800°C, respectively. As shown by Figure II-2, m_{150} consists
212 of the freshly formed brucite and the rest of MgO(s) (periclase) that did not react with DI water,
213 where n and FW denote the moles and formula mass (independent of heating)

214 $$m_{150} = n_{MgO(s)/150} \cdot FW_{MgO(s)} + n_{Mg(OH)2/150} \cdot FW_{Mg(OH)2} \quad (10)$$

215 m_{800} consists of the periclase resulting from brucite calcination and the periclase that did not react
216 with DI water. The law of mole conservation leads to:

217 $$m_{800} = n_{MgO(s)/800} \cdot FW_{MgO(s)} \quad (11)$$

218 Therefore, by subtracting Equation (11) from Equation (10):

219 $$m_{150} - m_{800} = (n_{MgO(s)/150} - n_{MgO(s)/800}) \cdot FW_{MgO(s)} + n_{Mg(OH)2/150} \cdot FW_{Mg(OH)2} \quad (12)$$

220 By the mass balance of Mg solids in Equation (13), Equation (12) can be rearranged into Equation
221 (14);

222 $$n_{MgO(s)/800} = n_{MgO(s)/150} + n_{Mg(OH)2/150} \quad (13)$$

223 $$m_{150} - m_{800} = (FW_{Mg(OH)2} - FW_{MgO(s)}) \cdot n_{Mg(OH)2/150} \quad (14)$$

224 Considering that $FW_{Mg(OH)2} - FW_{MgO(s)} = FW_{H2O}$, and $n_{Mg(OH)2/150} = n_{H2O}$;

225 $$n_{H2O} = n_{Mg(OH)2/150} = \frac{m_{150} - m_{800}}{FW_{H2O}} \quad (15)$$

Information Only

The accuracy of this LOI technique is based on the assumptions that (i) the paper filters (3 μm of pore size dimension) do not lose fine particles of $Mg(OH)_2(s)$ that may have formed during the hydration; (ii) the unbound water lingering in the filtered solids will not significantly contribute to MgO(s) hydration prior to heating in the LOI method; (iii) the 2-hour heating process at 150°C removes only the unbound water captured in the pore space without back-converting $Mg(OH)_2(s)$ to MgO(s); and (iv) the 3-hour heating at 800°C completes the conversion of $Mg(OH)_2(s)$ back to the MgO(s) by making $Mg(OH)_2(s)$ lose the H_2O in its structure (Deng et al., 2006b) .

The results of LOI measurements on the three size fractions (small, mixed, large) are reported in Sections II.1.5.1.1, II.1.5.1.2, and II.1.5.1.3. The individual LOI results are compared in Section II.1.6.1 (Figure II-9).

II.1.5.1.1. LOI results for Small Particles

LOI measurements of the **Small Particle** size fraction (S in the Sample ID in Table II-1) are summarized in Table II-1, and the data processing to calculate the mole fractions of $Mg(OH)_2(s)$ and MgO(s) is presented in Table II-2. The mole fractions are plotted in Figure II-3. The statistics of the mole fractions are tabulated in Table II-3 and plotted in Figure II-4.

Table II-1. Small size fraction: LOI measurements.

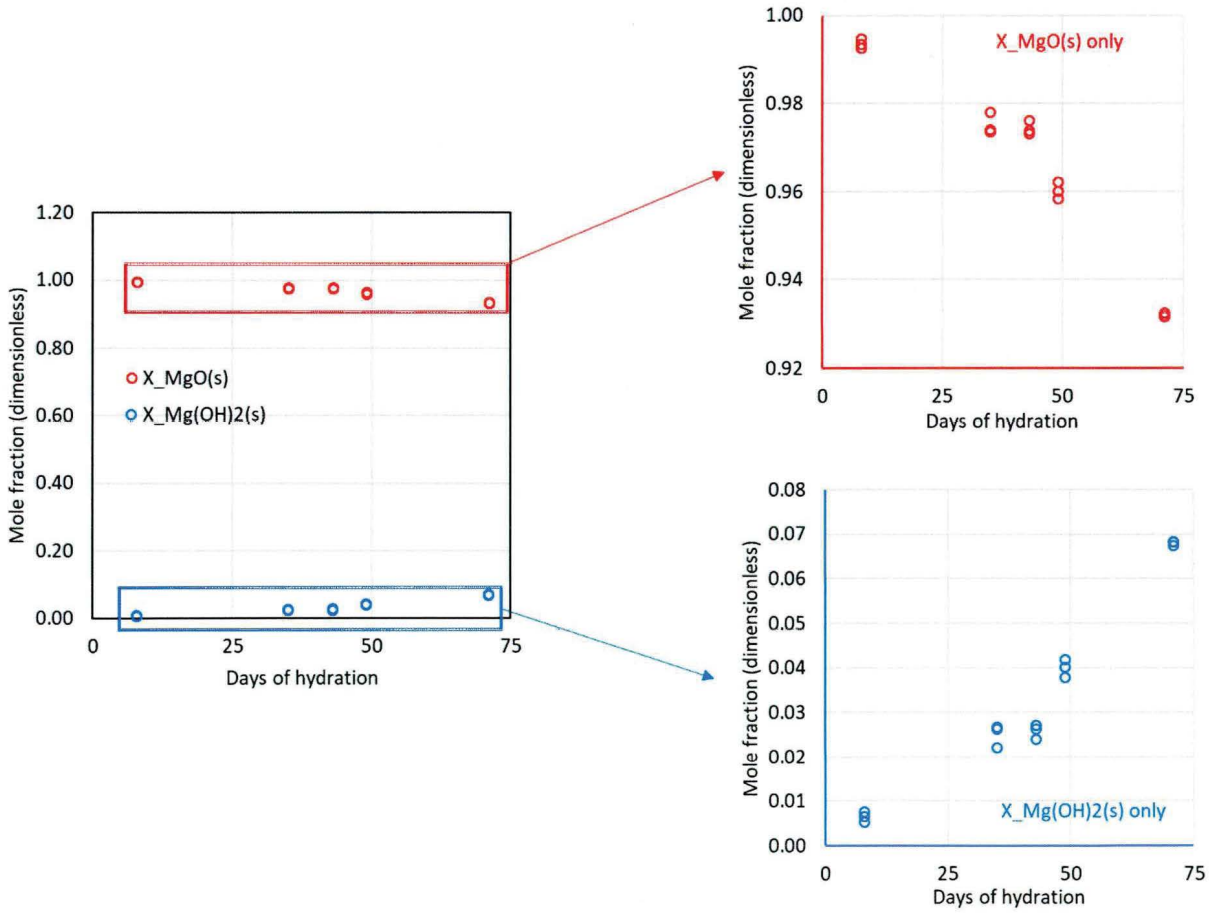
Sample ID	Start Date	Collection Date	Days of hydration	Before Heating Crucible mass (g)	Crucible + [MgO(s) + Mg(OH)2(s)+H2O] (g)	After 2 h. at 150°C Crucible + [MgO(s) + Mg(OH)2(s)] (g)	After 2 hrs. at 800°C Crucible + [MgO(s)] (g)	Source
DI-S-2-1-T1	8/16/2022	8/24/2022	8	33.34515	37.35282	36.94915	36.93712	WIPP-MM-MgO-23, page 79
DI-S-2-2-T1	8/16/2022	8/24/2022	8	39.81609	43.81946	43.43249	43.42399	WIPP-MM-MgO-23, page 79
DI-S-2-3-T1	8/16/2022	8/24/2022	8	38.07953	42.08905	41.61658	41.60621	WIPP-MM-MgO-23, page 79
DI-S-1-1-T1	6/7/2022	7/12/2022	35	33.34661	37.36820	36.91668	36.87537	WIPP-MM-MgO-23, page 72
DI-S-1-2-T1	6/7/2022	7/12/2022	35	39.81656	43.90923	43.23080	43.19069	WIPP-MM-MgO-23, page 72
DI-S-1-3-T1	6/7/2022	7/12/2022	35	38.07997	42.07716	40.98184	40.95359	WIPP-MM-MgO-23, page 72
DI-S-1-1-T2	6/7/2022	7/20/2022	43	33.34532	37.34300	36.81592	36.77559	WIPP-MM-MgO-23, page 73
DI-S-1-2-T2	6/7/2022	7/20/2022	43	39.81596	43.81672	43.28456	43.24793	WIPP-MM-MgO-23, page 73
DI-S-1-3-T2	6/7/2022	7/20/2022	43	38.07962	42.07409	41.54441	41.50304	WIPP-MM-MgO-23, page 73
DI-S-1-1-T3	6/7/2022	7/26/2022	49	33.34520	37.33994	36.92372	36.86069	WIPP-MM-MgO-23, page 74
DI-S-1-2-T3	6/7/2022	7/26/2022	49	39.81594	43.81786	43.39152	43.33203	WIPP-MM-MgO-23, page 74
DI-S-1-3-T3	6/7/2022	7/26/2022	49	38.07967	42.07990	41.52762	41.46443	WIPP-MM-MgO-23, page 74
DI-S-1-1-T4	6/7/2022	8/17/2022	71	33.34485	37.34485	36.89833	36.79305	WIPP-MM-MgO-23, page 77
DI-S-1-2-T4	6/7/2022	8/17/2022	71	39.81666	43.81462	43.39962	43.29472	WIPP-MM-MgO-23, page 77
DI-S-1-3-T4	6/7/2022	8/17/2022	71	38.08084	42.09584	41.64071	41.53538	WIPP-MM-MgO-23, page 77

Information Only

Table II-2. Small size fraction: Data processing to calculate the mole fractions of remaining MgO(s) and the formed $Mg(OH)_2(s)$ using equations in Section II.1.5.1.

Sample ID	Days of hydration	[MgO(s) + Mg(OH)2(s)] (g), no heating	[MgO(s) + Mg(OH)2(s)] (g), 2 hrs at 150°C	[MgO(s) + Mg(OH)2(s)] (g), 2 hrs at 800°C	gram H2O, bound	gram H2O in Mg(OH)2(s)	gram H2O total	mole Mg(OH)2(s)	mole MgO(s)	X_Mg(OH)2(s)	X_MgO(s)
DI-S-2-1-T1	8	4.0077	3.6040	3.5920	0.4037	0.0120	0.4157	6.68E-04	8.84E-02	0.007	0.993
DI-S-2-2-T1	8	4.0034	3.6164	3.6079	0.3870	0.0085	0.3955	4.72E-04	8.90E-02	0.005	0.995
DI-S-2-3-T1	8	4.0095	3.5371	3.5267	0.4725	0.0104	0.4828	5.76E-04	8.69E-02	0.007	0.993
DI-S-1-1-T1	35	4.0216	3.5701	3.5288	0.4515	0.0413	0.4928	2.29E-03	8.52E-02	0.026	0.974
DI-S-1-2-T1	35	4.0927	3.4142	3.3741	0.6784	0.0401	0.7185	2.23E-03	8.15E-02	0.027	0.973
DI-S-1-3-T1	35	3.9972	2.9019	2.8736	1.0953	0.0282	1.1236	1.57E-03	6.97E-02	0.022	0.978
DI-S-1-1-T2	43	3.9977	3.4706	3.4303	0.5271	0.0403	0.5674	2.24E-03	8.29E-02	0.026	0.974
DI-S-1-2-T2	43	4.0008	3.4686	3.4320	0.5322	0.0366	0.5688	2.03E-03	8.31E-02	0.024	0.976
DI-S-1-3-T2	43	3.9945	3.4648	3.4234	0.5297	0.0414	0.5711	2.30E-03	8.26E-02	0.027	0.973
DI-S-1-1-T3	49	3.9947	3.5785	3.5155	0.4162	0.0630	0.4793	3.50E-03	8.37E-02	0.040	0.960
DI-S-1-2-T3	49	4.0019	3.5756	3.5161	0.4263	0.0595	0.4858	3.30E-03	8.39E-02	0.038	0.962
DI-S-1-3-T3	49	4.0002	3.4480	3.3848	0.5523	0.0632	0.6155	3.51E-03	8.05E-02	0.042	0.958
DI-S-1-1-T4	71	4.0000	3.5535	3.4482	0.4465	0.1053	0.5518	5.84E-03	7.97E-02	0.068	0.932
DI-S-1-2-T4	71	3.9980	3.5830	3.4781	0.4150	0.1049	0.5199	5.82E-03	8.05E-02	0.067	0.933
DI-S-1-3-T4	71	4.0150	3.5599	3.4545	0.4551	0.1053	0.5605	5.85E-03	7.99E-02	0.068	0.932

Figure II-3. Small size fraction: Plots of the mole fractions in Table II-2.



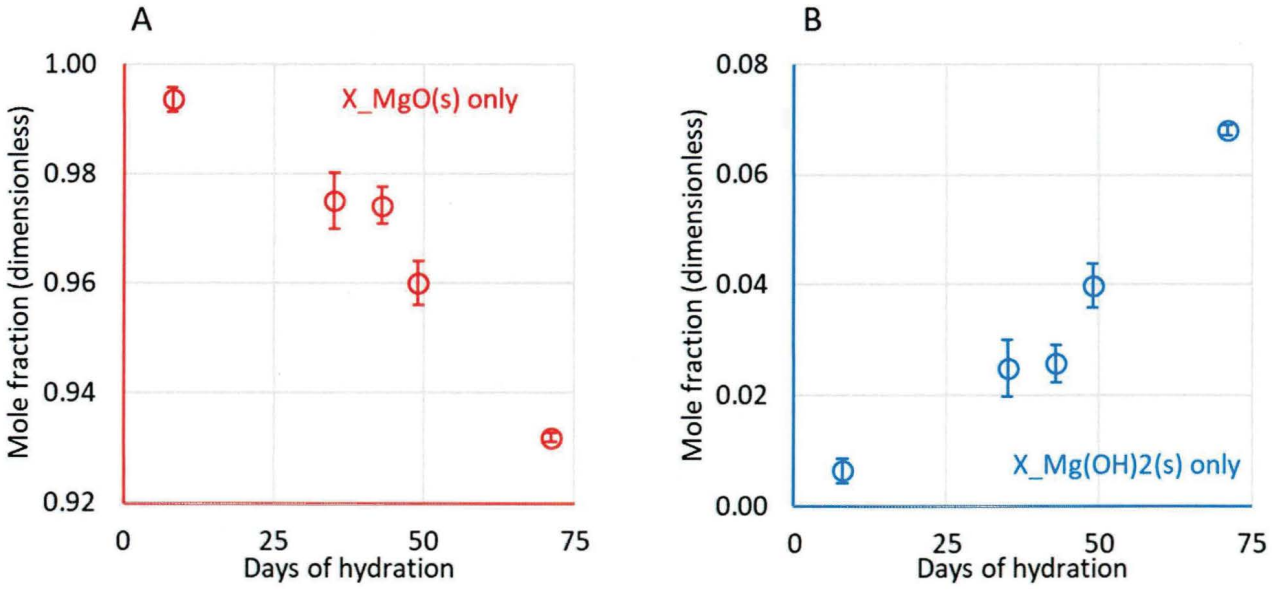
Information Only

Table II-3. Small size fraction: Statistics of the mole fractions in Table II-2 and Figure II-3.

Statistics	X_Mg(OH)2(s)				X_MgO(s)			
Days	Average	2SD	%2SD	Count	Average	2SD	%2SD	Count
8	0.006	0.002	35%	3	0.994	0.002	0%	3
35	0.025	0.005	20%	3	0.975	0.005	1%	3
43	0.026	0.003	13%	3	0.974	0.003	0%	3
49	0.040	0.004	10%	3	0.96	0.004	0%	3
71	0.068	0.001	1%	3	0.932	0.001	0%	3

Standard deviations are the same for both mole fractions because the $X_{MgO(s)}$ are calculated via Equation (9) on page 8 based on the measured $X_{Mg(OH)2(s)}$.

Figure II-4. Small size fraction: Plots of the statistics of the mole fractions in Table II-3.



As illustrated by Figure II-4, Small Size Particles are hydrated up to 7 % at 71 days of hydration. The data points at 7, 49 and 71 days of hydration time appear to be statistically different from other data points. Those at 35 and 43 days of hydration time have overlapping interval of confidence, suggesting that they are statistically similar to each other. Because we have a limited number of reactors, we could not keep stopping the aging every 7 days. Yet we did so, because the theory foresees that kinetics is the fastest at the beginning of the reaction. These observations eventually led to an increase in the time between reactor terminations.

Information Only

II.1.5.1.2. LOI results of Mixed Size Particles

LOI measurements of the **Mixed Size fraction** (M in the Sample ID in Table II-4) are summarized in Table II-4, and the data processing to calculate the mole fractions of $Mg(OH)_2(s)$ and MgO(s) is presented in Table II-5. The mole fractions are plotted in Figure II-5. The statistics of the mole fractions are tabulated in Table II-6 and plotted in Figure II-6.

Table II-4. Mixed-size fraction: LOI measurements.

Sample ID	Start Date	Collection Date	Days of hydration	Before Heating Crucible Mass (g)	Crucible + [MgO(s) + Mg(OH)2(s)] (g)	After 2 h. at 150°C Crucible + [MgO(s) + Mg(OH)2(s)] (g)	After 2 hrs. at 800°C Crucible + [MgO(s) + Mg(OH)2(s)] (g)	Source
DI-M-2-1-T1	8/16/2022	8/24/2022	8	39.10711	43.11845	42.79148	42.78264	WIPP-MM-MgO-23, page 79
DI-M-2-2-T1	8/16/2022	8/24/2022	8	35.80563	39.80205	39.45067	39.43930	WIPP-MM-MgO-23, page 79
DI-M-2-3-T1	8/16/2022	8/24/2022	8	43.50147	47.50559	47.22389	47.21415	WIPP-MM-MgO-23, page 79
DI-M-1-1-T1	6/7/2022	7/12/2022	35	38.54005	42.55171	41.83512	41.80249	WIPP-MM-MgO-23, page 72
DI-M-1-2-T1	6/7/2022	7/12/2022	35	34.30615	38.33070	37.49669	37.45571	WIPP-MM-MgO-23, page 72
DI-M-1-3-T1	6/7/2022	7/12/2022	35	43.50161	47.55378	46.69990	46.66232	WIPP-MM-MgO-23, page 72
DI-M-1-1-T2	6/7/2022	7/20/2022	43	38.53977	42.54500	42.05223	42.00927	WIPP-MM-MgO-23, page 73
DI-M-1-2-T2	6/7/2022	7/20/2022	43	34.30716	38.30438	37.90323	37.85379	WIPP-MM-MgO-23, page 73
DI-M-1-3-T2	6/7/2022	7/20/2022	43	43.50267	47.50086	47.13626	47.09291	WIPP-MM-MgO-23, page 73
DI-M-1-1-T3	6/7/2022	7/26/2022	49	38.53956	42.53964	42.15366	42.09703	WIPP-MM-MgO-23, page 74
DI-M-1-2-T3	6/7/2022	7/26/2022	49	34.30590	38.30952	37.81355	37.75752	WIPP-MM-MgO-23, page 74
DI-M-1-3-T3	6/7/2022	7/26/2022	49	43.50132	47.50550	47.04123	46.98731	WIPP-MM-MgO-23, page 74
DI-M-1-1-T4	6/7/2022	8/17/2022	71	39.11709	43.09379	42.60800	42.50275	WIPP-MM-MgO-23, page 77
DI-M-1-2-T4	6/7/2022	8/17/2022	71	35.80555	39.78201	39.26275	39.17062	WIPP-MM-MgO-23, page 77
DI-M-1-3-T4	6/7/2022	8/17/2022	71	43.50167	47.49511	46.88220	46.78467	WIPP-MM-MgO-23, page 77

Table II-5. Mixed-size fraction: Data processing to calculate the mole fractions of remaining MgO(s) and the formed $Mg(OH)_2(s)$ using equations in Section II.1.5.1.

Sample ID	Days of hydration	[MgO(s) + Mg(OH)2(s)] (g), no heating	[MgO(s) + Mg(OH)2(s)] (g), 2 hrs at 150°C	[MgO(s) + Mg(OH)2(s)] (g), 2 hrs at 800°C	gram H2O, bound	gram H2O in Mg(OH)2 (s)	gram H2O total	mole Mg(OH)2 (s)	mole MgO(s)	X_Mg(OH)2(s)	X_MgO(s)
DI-M-2-1-T1	8	4.0113	3.6844	3.6755	0.3270	0.0088	0.3358	4.91E-04	9.07E-02	0.005	0.995
DI-M-2-2-T1	8	3.9964	3.6450	3.6337	0.3514	0.0114	0.3627	6.31E-04	8.95E-02	0.007	0.993
DI-M-2-3-T1	8	4.0041	3.7224	3.7127	0.2817	0.0097	0.2914	5.41E-04	9.16E-02	0.006	0.994
DI-M-1-1-T1	35	4.0117	3.2951	3.2624	0.7166	0.0326	0.7492	1.81E-03	7.91E-02	0.022	0.978
DI-M-1-2-T1	35	4.0246	3.1905	3.1496	0.8340	0.0410	0.8750	2.27E-03	7.59E-02	0.029	0.971
DI-M-1-3-T1	35	4.0522	3.1983	3.1607	0.8539	0.0376	0.8915	2.09E-03	7.63E-02	0.027	0.973
DI-M-1-1-T2	43	4.0052	3.5125	3.4695	0.4928	0.0430	0.5357	2.38E-03	8.37E-02	0.028	0.972
DI-M-1-2-T2	43	3.9972	3.5961	3.5466	0.4012	0.0494	0.4506	2.74E-03	8.52E-02	0.031	0.969
DI-M-1-3-T2	43	3.9982	3.6336	3.5902	0.3646	0.0433	0.4080	2.41E-03	8.67E-02	0.027	0.973
DI-M-1-1-T3	49	4.0001	3.6141	3.5575	0.3860	0.0566	0.4426	3.14E-03	8.51E-02	0.036	0.964
DI-M-1-2-T3	49	4.0036	3.5077	3.4516	0.4960	0.0560	0.5520	3.11E-03	8.25E-02	0.036	0.964
DI-M-1-3-T3	49	4.0042	3.5399	3.4860	0.4643	0.0539	0.5182	2.99E-03	8.35E-02	0.035	0.965
DI-M-1-1-T4	71	3.9767	3.4909	3.3857	0.4858	0.1052	0.5910	5.84E-03	7.81E-02	0.070	0.930
DI-M-1-2-T4	71	3.9765	3.4572	3.3651	0.5193	0.0921	0.6114	5.11E-03	7.84E-02	0.061	0.939
DI-M-1-3-T4	71	3.9934	3.3805	3.2830	0.6129	0.0975	0.7104	5.41E-03	7.60E-02	0.066	0.934

Information Only

Figure II-5. Mixed-size fraction: Plots of the mole fractions in Table II-5.

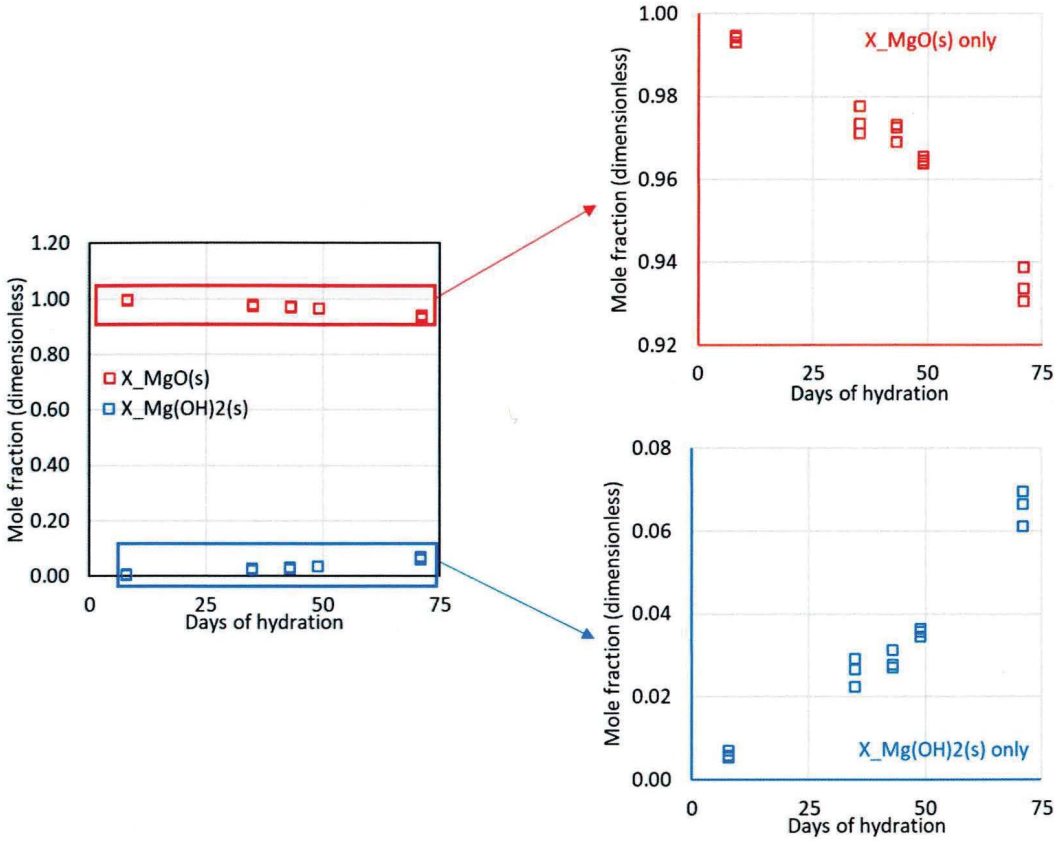


Table II-6. Mixed-size fraction: Statistics of the mole fractions in Table II-5 and Figure II-5.

Statistics	X_Mg(OH)2(s)				X_MgO(s)			
Days	Average	2SD	%2SD	Counts	Average	2SD	%2SD	Counts
8	0.006	0.002	27%	3	0.994	0.002	0%	3
35	0.026	0.007	23%	3	0.974	0.007	1%	3
43	0.029	0.004	16%	3	0.971	0.004	0%	3
49	0.036	0.002	5%	3	0.964	0.002	0%	3
71	0.066	0.008	13%	3	0.934	0.008	1%	3

Standard deviations are the same for both mole fractions because the $X_{MgO(s)}$ are calculated via Equation (9) based on the measured $X_{Mg(OH)2(s)}$.

Information Only

Figure II-6. Mixed-size fraction: Plots of the statistics of the mole fractions in Table II-6.

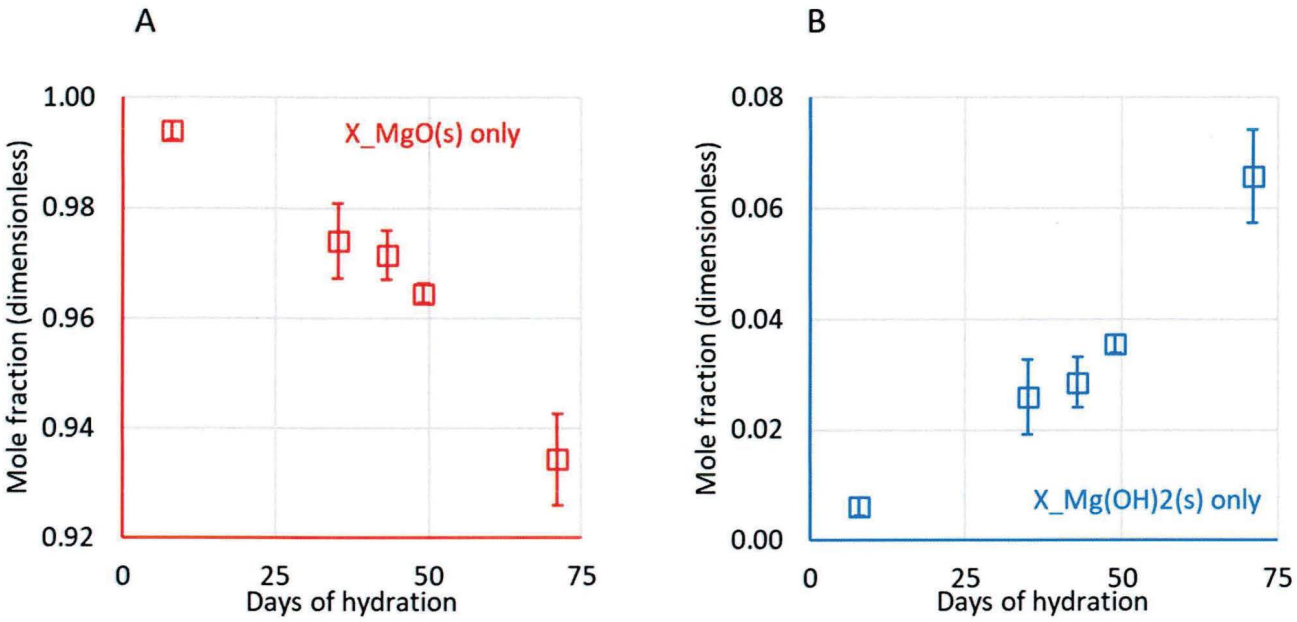


Figure II-6 illustrates that mixed size particles are hydrated up to 7% after 71 days. The data point at 7 and 71 days of hydration time are statistically different from other data points. Those at 35, 43 and 49 days of hydration time have overlapping interval of confidence, suggesting that they are statistically similar to each other. Because we have a limited number of reactors, we could not keep stopping the aging every 7 days. Yet we did so, because the theory foresees that kinetics is the fastest at the beginning of the reaction. These observations eventually led us to increase the time between reactor terminations.

II.1.5.1.3. LOI results of Large Size Particles

LOI measurements of the **Large Size Particle** (L in the Sample ID in Table II-7) are summarized in Table II-7, and the data processing to calculate the mole fractions of $Mg(OH)_2(s)$ and MgO(s) are presented in Table II-8. The mole fractions are plotted in Figure II-7. The statistics of the mole fractions are tabulated in Table II-9 and plotted in Figure II-8.

Table II-7. Large size fraction: LOI measurements.

Sample ID	Start Date	Collection Date	Days of hydration	Before Heating Crucible Mass (g)	Crucible + [MgO(s) + Mg(OH)2(s)] (g)	After 2 h. at 150°C Crucible + [MgO(s) + Mg(OH)2(s)] (g)	After 2 hrs. at 800°C Crucible + [MgO(s) + Mg(OH)2(s)] (g)	Source
DI-L-2-1-T1	8/16/2022	8/24/2022	8	34.30546	38.30067	37.68392	37.67847	WIPP-MM-MgO-23, page 79
DI-L-2-2-T1	8/16/2022	8/24/2022	8	32.35415	36.35162	35.80226	35.79650	WIPP-MM-MgO-23, page 79
DI-L-2-3-T1	8/16/2022	8/24/2022	8	37.49256	41.49701	40.88205	40.87600	WIPP-MM-MgO-23, page 79
DI-L-1-1-T1	6/7/2022	7/12/2022	35	36.86344	40.82646	40.43589	40.40559	WIPP-MM-MgO-23, page 72
DI-L-1-2-T1	6/7/2022	7/12/2022	35	35.80630	39.82119	39.51802	39.48763	WIPP-MM-MgO-23, page 72

Information Only

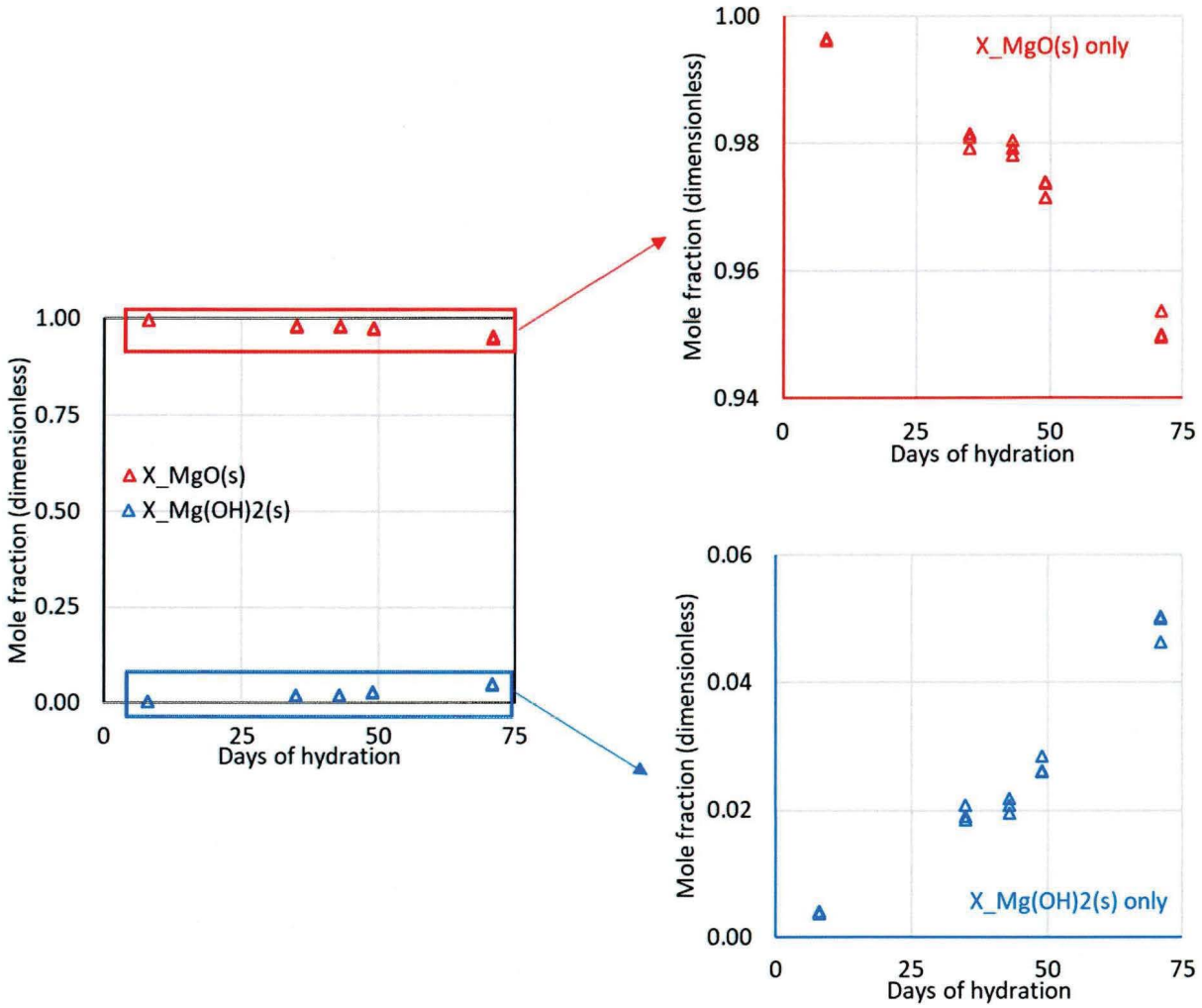
DI-L-1-3-T1	6/7/2022	7/12/2022	35	37.49289	41.58192	41.23031	41.19591	WIPP-MM-MgO-23, page 72
DI-L-1-1-T2	6/7/2022	7/20/2022	43	36.86341	40.86611	40.27772	40.24815	WIPP-MM-MgO-23, page 73
DI-L-1-2-T2	6/7/2022	7/20/2022	43	35.80593	39.80137	39.25188	39.22005	WIPP-MM-MgO-23, page 73
DI-L-1-3-T2	6/7/2022	7/20/2022	43	37.49278	41.49846	41.01390	40.97983	WIPP-MM-MgO-23, page 73
DI-L-1-1-T3	6/7/2022	7/26/2022	49	32.92137	36.92692	36.40595	36.36200	WIPP-MM-MgO-23, page 74
DI-L-1-2-T3	6/7/2022	7/26/2022	49	35.80590	39.82384	39.30461	39.26396	WIPP-MM-MgO-23, page 74
DI-L-1-3-T3	6/7/2022	7/26/2022	49	37.49287	41.49948	41.04698	41.00610	WIPP-MM-MgO-23, page 74
DI-L-1-1-T4	6/7/2022	8/17/2022	71	34.30556	38.28598	37.68596	37.61144	WIPP-MM-MgO-23, page 77
DI-L-1-2-T4	6/7/2022	8/17/2022	71	32.35423	36.34796	35.73410	35.66542	WIPP-MM-MgO-23, page 77
DI-L-1-3-T4	6/7/2022	8/17/2022	71	37.49285	41.51459	40.93715	40.86172	WIPP-MM-MgO-23, page 77

Table II-8. Large size fraction: Data processing to calculate the mole fractions of remaining MgO(s) and the formed $Mg(OH)_2(s)$ using equations in Section II.1.5.1.

Sample ID	Days of hydration	[MgO(s) + Mg(OH)2(s)] (g), no heating	[MgO(s) + Mg(OH)2(s)] (g), 2 hrs at 150°C	[MgO(s) + Mg(OH)2(s)] (g), 2 hrs at 800°C	gram H2O, bound	gram H2O in Mg(OH)2(s)	gram H2O total	mole Mg(OH)2(s)	mole MgO(s)	X_Mg(OH)2(s)	X_MgO(s)
DI-L-2-1-T1	8	3.9952	3.3785	3.3730	0.6167	0.0055	0.6222	3.03E-04	8.34E-02	0.004	0.996
DI-L-2-2-T1	8	3.9975	3.4481	3.4424	0.5494	0.0058	0.5551	3.20E-04	8.51E-02	0.004	0.996
DI-L-2-3-T1	8	4.0045	3.3895	3.3834	0.6150	0.0061	0.6210	3.36E-04	8.36E-02	0.004	0.996
DI-L-1-1-T1	35	3.9630	3.5725	3.5422	0.3906	0.0303	0.4209	1.68E-03	8.62E-02	0.019	0.981
DI-L-1-2-T1	35	4.0149	3.7117	3.6813	0.3032	0.0304	0.3336	1.69E-03	8.96E-02	0.018	0.982
DI-L-1-3-T1	35	4.0890	3.7374	3.7030	0.3516	0.0344	0.3860	1.91E-03	9.00E-02	0.021	0.979
DI-L-1-1-T2	43	4.0027	3.4143	3.3847	0.5884	0.0296	0.6180	1.64E-03	8.23E-02	0.020	0.980
DI-L-1-2-T2	43	3.9954	3.4460	3.4141	0.5495	0.0318	0.5813	1.77E-03	8.29E-02	0.021	0.979
DI-L-1-3-T2	43	4.0057	3.5211	3.4871	0.4846	0.0341	0.5186	1.89E-03	8.46E-02	0.022	0.978
DI-L-1-1-T3	49	4.0056	3.4846	3.4406	0.5210	0.0439	0.5649	2.44E-03	8.29E-02	0.029	0.971
DI-L-1-2-T3	49	4.0179	3.4987	3.4581	0.5192	0.0406	0.5599	2.26E-03	8.35E-02	0.026	0.974
DI-L-1-3-T3	49	4.0066	3.5541	3.5132	0.4525	0.0409	0.4934	2.27E-03	8.49E-02	0.026	0.974
DI-L-1-1-T4	71	3.9804	3.3804	3.3059	0.6000	0.0745	0.6745	4.14E-03	7.79E-02	0.050	0.950
DI-L-1-2-T4	71	3.9937	3.3799	3.3112	0.6139	0.0687	0.6825	3.81E-03	7.83E-02	0.046	0.954
DI-L-1-3-T4	71	4.0217	3.4443	3.3689	0.5774	0.0754	0.6529	4.19E-03	7.94E-02	0.050	0.950

Information Only

302 Figure II-7. Large size fraction: Plots of the mole fractions in Table II-8.



303

304 Table II-9. Large size fraction: Statistics of the mole fractions in Table II-8 and Figure
305 II-7.

Statistics	X_Mg(OH)2(s)				X_MgO(s)			
Days	Average	2SD	%2SD	Counts	Average	2SD	%2SD	Counts
8	0.004	3.93E-04	5%	3	0.996	3.93E-04	0%	3
35	0.019	0.002	12%	3	0.981	0.002	0%	3
43	0.021	0.002	14%	3	0.979	0.002	0%	3
49	0.027	0.003	9%	3	0.973	0.003	0%	3
71	0.049	0.004	9%	3	0.951	0.004	0%	3

306

307 Standard deviations are the same for both mole fractions because the $X_{MgO(s)}$ are calculated via
308 Equation (9) on based on the measured $X_{Mg(OH)2(s)}$.

309

Information Only

Figure II-8. Large size fraction: Plots of the statistics of the mole fractions in Table II-9.

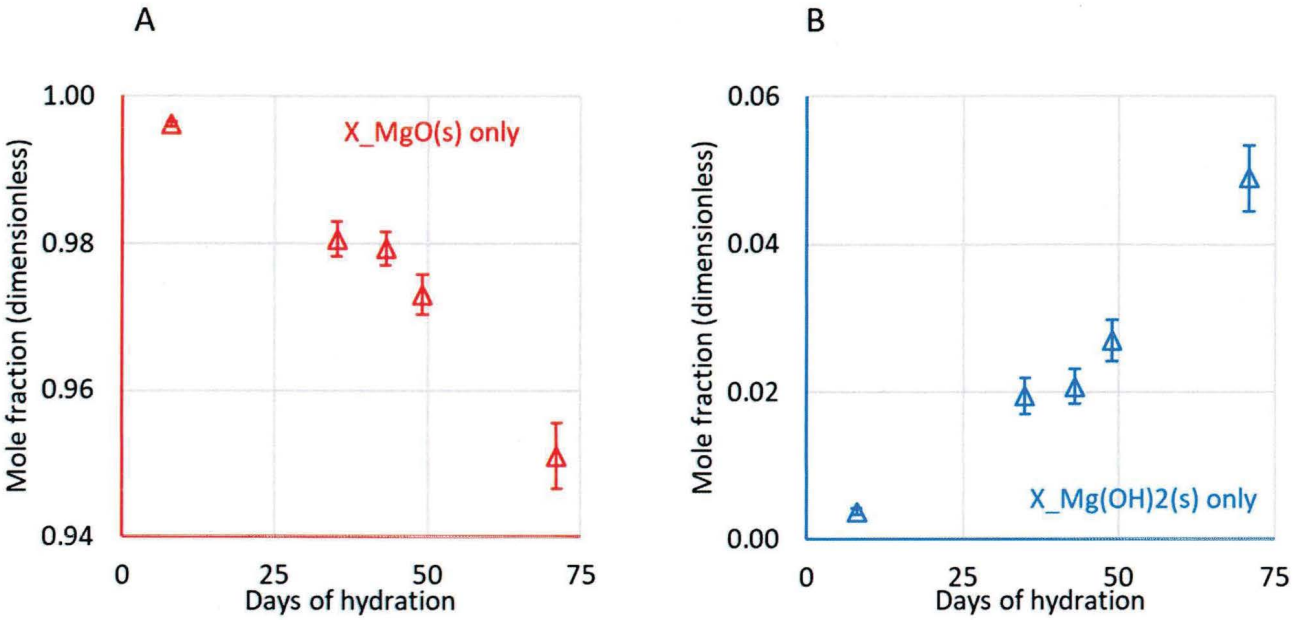


Figure II-8 illustrates that large size particles are hydrated up to 5% after 71 days. The data point at 7, 49 and 71 days of hydration time are statistically different from other data points. Those at 35 and 43 days of hydration time have overlapping interval of confidence, suggesting that they are statistically similar to each other. These observations eventually led to increase the time between two reactors termination.

II.1.6. Observations

II.1.6.1. LOI

We made macroscopic observation of the hydrated MgO(s) sample. Overall, all samples of all particle sizes that hydrated up to 43 days maintained the initial granularity with no sign of cementing or caking. The large particles that aged for more than 49 days did not exhibit any significant change of aspect either, remaining disaggregated spherical particles. A portion of the small and mixed size particle batches exhibited minor aggregation after 49 days of aging however the overall aspect remained unchanged. After drying in the desiccator overnight there was no need to crush the samples as they were easy to manipulate. No cementing was observed as was expected for MM MgO hydrated in only DI water.

Figure II-9 exhibits an overlay of the mole fractions obtained by LOI for all particle sizes. Visually, it is observed that at 7 days of aging time, the different particle sizes show no statistical difference in terms of extent of hydration. Visually, we observe that at 35 and 43 days of aging, errors bars

Information Only

overlap each other, suggesting no statistical difference. Starting at 50 days of hydration the large particle size began to exhibit a statistically different extent of hydration (error bars not overlaying any other) from small and mixed particle sizes. Though it is too soon to confirm, it seems this difference would increase as the experiments progress, following the observations made by Deng et al. (2007b). The extent of hydration increases as particle size fraction of MM MgO decreases. This observation supports the hypothesis: the larger the particle, the slower the hydration rate due to low surface area. The surface areas have not been measured at the date of this report. BET (Brunauer-Emmett-Teller) surface area measurements for particle size batch will be reported in the next revision.

Potential biases of LOI include the following:

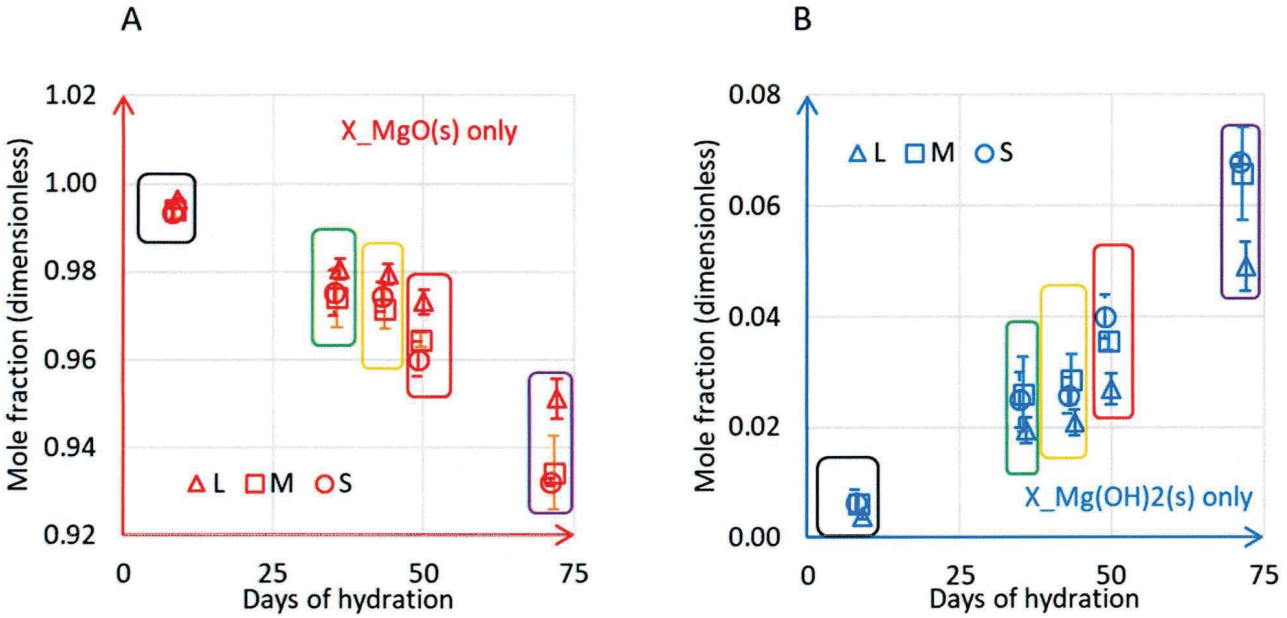
- There is no information about the potential variation of mass of the crucible after being heated up to 800°C.

- The temperature difference between unbound and bound water was defined based on similar experiments performed in Smithson and Bakhshi (1969), Snider (2003), Wall (2005) and Huang et al. (2020). A Thermogravimetric analysis (TGA) of a commercial, standard $Mg(OH)_2(s)$ could be a tool to elucidate this potential bias. As suggested by Deng et al (2006a) the current T = 150°C is set to differentiate the pore water from crystalline water of brucite. T = 800°C provide enough heat to convert brucite to periclase.

Figure II-9. Overlay of the mole fractions obtained by LOI. A: Overlay of Figure II-4A, Figure II-6A, and Figure II-8A. B: Overlay of Figure II-4B, Figure II-6B, and Figure II-8B. Days of hydration are the same as in Figure II-4, Figure II-6, and Figure II-8. They are staggered for clarity in the Figures below, i.e., black

Information Only

rectangles: 8 days, green rectangles: 35 days, yellow rectangles: 43 days, red rectangles: 49 days, violet rectangles: 71 days.



II.1.7. Model Parameterization

II.1.7.1. LOI

The sampling period must be expanded by several months before a rate constant can be derived. In the coming months, SNL WIPP Geochemistry will establish a better understanding of the time frame to which the sampling period should be extended. LOI measures the loss of mass from unbound water and the mass of bound water derived from $Mg(OH)_2(s)$. The precision for the $X_{MgO(s)}$, i.e., 2SDs in Tables, is calculated to be the same as the precision of $X_{Mg(OH)2(s)}$ because of the application of Equation (9) to calculate the $X_{MgO(s)}$. An uncertainty propagation model can be applied to establish statistically rigorous precision to the $X_{MgO(s)}$, which will be performed in the next Revision of this report (when more time-dependent measurements are available).

II.1.8. Summary

At the time of this Revision, the final goal of this study has not been achieved as the remaining samples require more aging time to determine the rate constant.

It is too soon to confirm or refute the hypotheses listed at the beginning of this report due to lack of data.

Information Only

H-1 (*The hydration of MgO(s) in water can be described by Reaction (1), and the sole product is $Mg(OH)_2(s)$*): Supplementary XRD data (absent in this report – though they are recorded in SN pages, they were not reviewed yet under SNL WIPP QA at the time this report was written) exhibited that hydrated samples contained traces of brucite with a dominant periclase signal. This suggests hydration is too low to observe strong brucite signal on the XRD pattern. It also confirms (so far) that brucite is the only product of the MgO(s) hydration reaction and that Reaction (1) goes in the direction of forming brucite.

H-2 (*Because of kinetics, Reaction (1) would not go to completion in any near future in the presence of excess water*): Confirming this hypothesis require the acquisition of more data. At the time this report is written, mole fractions did not reach a plateau that would indicate that the hydration would not go to completion. ICP-AES measurement have not been yet performed to confirm the theoretical dissolved Mg concentration and pH.

H-3 (*The hydration reaction rate can be parameterized by first order reaction kinetics*): Once again, the number of data acquired so far is deemed not enough to allow us to determine the rate equation and thus the order. This hypothesis will be discussed in future revisions.

H-4 (*It is assumed that hydration rate is dependent of the specific surface area (SSA) of the MgO(s) particles*): The results presented in this report show a discrimination with time between size particles. The largest particles tend to hydrate slower than the small and mixed size particles, suggesting specific surface area may play a role in hydration kinetics. More data are needed to confirm these tendencies and this hypothesis. Depending on the future, result we might be able to identify the existence of several hydration process as suggested by Deng et al. (2007ab).

However, given how slow MgO(s) hydrates, it is safe to declare that the LOI method assumption and hypothesis H-2 (see II.1.2) is correct so far.

II.2. Future Work - Hydration

The MgO(s) - H_2O experiment of this revision is included in a multi-year experimental plan which has the final goal of determining MgO(s) hydration rates in WIPP relevant brines. To accomplish this goal, it is necessary to first complete this task in simple systems and then proceed in increasingly complex brines by introducing WIPP relevant salts. Table II-10 summarized the different MgO(s) hydration experiments that will be investigated and their respective time schedule.

Information Only

Table II-10. System to be investigated for MgO(s) hydration and their scheduled time of completion. (Italic font is a tentative schedule of the experimental plan and is subject to change)

System	Scheduled
MgO(s) – H_2O	To be completed by September 2023
MgO(s) - NaCl - H_2O	To be completed by December 2024
MgO(s) - $MgCl_2$ - H_2O	*To be completed by June 2024*
MgO(s) - $MgCl_2$ - NaCl - H_2O	*To be completed by December 2025*
MgO(s) - GWB	*To be completed by September 2026*
MgO(s) – H2O(g)	*To be completed by September 2027*

III. CARBONATION EXPERIMENTS

In later Revisions of this report, carbonation experiments using CO_2(g) will be presented (Table III-1) as a precursor to inundated carbonation experiments to isolate carbonation only. In inundated experiments, hydration and carbonation would proceed simultaneously. The results of carbonation of MgO(s) by CO_2(g) in the absence of liquid water will be useful to characterize the competition between carbonation and hydration of MgO(s) in carbonated solutions.

Table III-1. System to be investigated for MgO(s) carbonation and their scheduled time of completion. (Italic font is a tentative schedule of the experimental plan and is subject to change)

System	Scheduled
MgO(s) – CO_2(g)	*To be completed by September 2025*
MgO(s) – $Na_{(2-x)}H_xCO_3$ - H_2O	*To be completed by September 2025*

Information Only

IV. CONCLUSIONS

This revision exhibits the preliminary results of a multi-year experimental plan whose goal is to determine the hydration and carbonation of MM MgO particles used in the WIPP repository. Future data are expected by the end of FY23.

The hypotheses described in Section II.1.2 cannot be fully confirmed yet, due to a lack of data, but will be addressed in the next revisions of this report.

Source of the uncertainties such as the loss of colloidal particles during 3 μm filtration, and uncertainties related to the temperature of calcination will also be addressed in the next Revision and dealt with accordingly. Likewise, the accuracy of LOI was based on the fact that the unbound water lingering in the filtered solids, will not significantly contribute to MgO(s) hydration prior to heating in the LOI method. This leads to uncertainty about when in time hydration actually stopped. Horizontal error bars could be added in future revisions to address this problem. As explained in the previous sections, we expect those processes to have little to no influence on the hydration rate, as their contribution is negligible.

V. ACKNOWLEDGMENT

Three reviews were conducted and documented under SNL WIPP QA. Technical review was performed by Martin Nemer, who independently verified the data processing in Table II-1 and Table II-2, QA review by Shelly Nielsen and Management review by Chammi Miller. Comments and the resolutions are documented. The authors thank reviewers for constructive comments. The authors are grateful to Randall Arnold, Heather Burton, and Grace Castle for the experimental work provided in the laboratory.

VI. REFERENCES

VI.1. A

Amaral, L. F., Oliveira, I. R., Salomão, R., Frollini, E., & Pandolfelli, V. C. (2010). Temperature and common-ion effect on magnesium oxide (Mgo) hydration. Ceramics International, 36(3), 1047–1054.

VI.2. B

Bratton, R.J. and G.W. Brindley. 1964. "Kinetics of Vapour Phase Hydration of Magnesium Oxide Part 2.-Dependence on Temperature and Water Vapour Pressure." Transactions of the Faraday Society, vol. 61, no. 509P, pp 1017-1025.

Information Only

VI.3. C

Chemical Rubber Company. 2003. CRC handbook of chemistry and physics: A ready-reference book of chemical and physical data (D. R. Lide, Ed.; 84. ed., 2003/2004). CRC Press.

VI.4. D

Deng, H., Y. Xiong, M. Nemer. 2006a. "Experimental Study of MgO Reaction Pathways and Kinetics Rev.0." TP 06-03, Revision 0. Carlsbad, NM: Sandia National Laboratories. ERMS 543433.

Deng, H., Y. Xiong, M. Nemer. 2007a. "Experimental Study of MgO Reaction Pathways and Kinetics Rev.1." TP 06-03, Revision 1. Carlsbad, NM: Sandia National Laboratories. ERMS 545182.

Deng, H. 2010. "Analysis of MgO Hydration and Carbonation Test Results, Analysis Plan AP-108, Rev. 1" Carlsbad, NM: Sandia National Laboratories. ERMS 553134.

Deng, H., Johnsen, S., Xiong, Y., Roselle, G.T. and Nemer, M. 2006b. Analysis of Martin Marietta MagChem 10 WTS-60. Carlsbad, NM: Sandia National Laboratories. ERMS 544712.

Deng, H., Xiong, Y. and Nemer, M. 2007b. Experimental study of MgO reaction pathways and Kinetics Rev 1. Carlsbad, NM: Sandia National Laboratories. ERMS 545182.

Deng, H., Johnsen, S., Xiong, Y. and Nemer, M. 2009. Experimental Work Conducted on MgO Long-Term Hydration: 2008 Milestone Report. Carlsbad, NM: Sandia National Laboratories. ERMS 551421

VI.5. G

Giauque, W. F., and Archibald, R. C., 1937. The entropy of water from third law of thermodynamics. The dissociation pressure and calorimetric heat of reaction Mg(OH)2 = MgO + H2O. The heat capacities of $Mg(OH)_2$ and MgO from 200 to 3000 K.: Jour. Am. Chem. Soc., v. 59, p. 561-569.

Ginstling, A. M. and Brounshtein, V. I. 1950. Concerning the Diffusion Kinetics of Reactions in Spherical Particles," J. Appl. ChcilL USSR, Vol. 23, 1950, pp. 1327-1338.

VI.6. H

Harvie, C. E., Møller, N., & Weare, J. H. 1984. The prediction of mineral solubilities in natural waters: The na-k-mg-ca-h-cl-so4-oh-hco3-co3-co2-h2o system to high ionic strengths at 25°c. Geochimica et Cosmochimica Acta, 48(4), 723–751.

Information Only

Huang, L., Yang, Z., & Wang, S. 2020. Influence of calcination temperature on the structure and hydration of MgO. Construction and Building Materials, 262, 120776.

VI.7. J

Jander, W. (1927). Reactions in the Solid State at High Temperatures. Zeitschrift Für Anorganische Und Allgemeine Chemie, 163(1), 1–30.

VI.8. K

Kitamura A., Onizuka K., Tanaka K. 1995. Hydration characteristics of magnesia, Taikabutsu Overseas 16 (3) 3–11.

VI.9. L

Layden, G. K., & Brindley, G. W. (1963). Kinetics of vapor-phase hydration of magnesium oxide. Journal of the American Ceramic Society, 46(11), 518–522.

Levenspiel, O. 1963. "Chemical Reaction Engineering," John Wiley & Sons, Inc., New York, pp 348-350.

VI.10. M

Martin Marietta Magnesia Specialties LLC, Composition certificate of MagChem 10. Sandia National Laboratories, Carlsbad, NM. ERMS 544635.

VI.11. N

Nowak E.J. 2003. “Analysis of MgO Hydration and Carbonation Test Results, Analysis Plan AP-108, Rev. 0”. Sandia National Laboratories, Carlsbad, NM. ERMS 530544.

VI.12. S

Smithson G.L., Bakhshi N.N., 1969. “The kinetics and mechanism of the hydration of magnesium oxide in a batch reactor”, Can. J. Chem. Eng. 47 508–513.

Snider, A.C., Y.-L. Xiong, 2002. "Experimental Study of WIPP Engineered Barrier MgO at Sandia National Laboratories Carlsbad Facility." TP 00-07, Rev. 2. Carlsbad, NM: Sandia National Laboratories. ERMS 523957.

Snider, A.C. 2003. Hydration of Magnesium Oxide in the Waste Isolation Pilot Plant. Material Research Society. Symp. Proc. Vol. 757.

Information Only

Snider, A.C., Y.-L. Xiong, and N.A. Wall. 2004. "Experimental Study of WIPP Engineered Barrier MgO at Sandia National Laboratories Carlsbad Facility." TP 00-07, Rev. 3. Carlsbad, NM: Sandia National Laboratories. ERMS 536591.

VI.13. T

Taylor, K., and Wells, L., 1938, Studies of the heat of solution of calcium and magnesium oxides and hydroxides: Jour. Research Natl. Bur. Standards, v. 21, p. 133-149.

VI.14. U

U.S. DOE. 2004. Title 40 CFR Part 191 Compliance Recertification Application for the Waste Isolation Pilot Plant, Vol. 1-8. DOE/WIPP 2004-3231. Carlsbad, NM: U.S. Department of Energy Carlsbad Field Office.

U.S. Department of Energy (DOE). 2019. Title 40 CFR Part 191 Subparts B and C Compliance Recertification Application 2019 for the Waste Isolation Pilot Plant, Appendix MgO-2019 Magnesium Oxide as an Engineered Barrier, Carlsbad, NM: Carlsbad Field Office. DOE/WIPP-19-3609, Rev 0.

U.S. EPA. 1998. "40 CFR 194, Criteria for the Certification and Recertification of the Waste Isolation Pilot Plant's Compliance With the Disposal Regulations. Certification Decision: Final Rule," Federal Register. Vol. 63, 27354-27406. Washington, DC: U.S. EPA Office of Radiation and Indoor Air.

VI.15. W

Wall, N. A. 2005. Preliminary Results for the Evaluation of Potential New MgO. Carlsbad, NM: Sandia National Laboratories. ERMS 538514.

VI.16. X

Xiong, Y., Deng, H., Nemer, M., & Johnsen, S. 2010. Experimental determination of the solubility constant for magnesium chloride hydroxide hydrate ($Mg_3Cl(OH)_5 \cdot 4H_2O$, phase 5) at room temperature, and its importance to nuclear waste isolation in geological repositories in salt formations. Geochimica et Cosmochimica Acta, 74(16), 4605–4611.

Information Only